Available online at www.sciencedirect.com
ScienceDirect
Journal of the Mechanics and Physics of Solids
55 (2007) 2237–2264

JOURNAL OF THE MECHANICS AND PHYSICS OF SOLIDS

www.elsevier.com/locate/jmps

Hyperelasticity with softening for modeling materials failure

K.Y. Volokh

Faculty of Civil and Environmental Engineering, Technion-I.I.T., Haifa 32000, Israel

Received 9 January 2007; received in revised form 25 February 2007; accepted 28 February 2007

Abstract

Traditional hyperelastic models of materials allow for the unlimited increase of the strain energy under the strain increase. It is clear, however, that no real material can accumulate the energy unlimitedly sustaining large enough strains. In the present work, we introduce a limiter for the strain energy—the critical failure energy, which can be interpreted as a failure constant characterizing the material 'toughness'. We show that the critical failure energy controls materials softening. The softening can enrich any existing model of the intact material with a failure description. We demonstrate the efficiency of the softening hyperelasticity approach on a variety of analytically tractable boundary value problems with a variety of material models. The proposed softening hyperelasticity approach is a possible alternative to the simplistic pointwise failure criteria of strength of materials on the one hand and the sophisticated approach of damage mechanics involving internal variables on the other hand.

Keywords: Biological material; Finite strain; Fracture; Hyperelastic material; Material failure

1. Introduction

Traditional hyperelastic models of materials allow for the unlimited increase of strain energy under the strain increase. It is clear, however, that no real material can sustain large enough strains. To account for the material failure a phenomenological approach of damage mechanics has been developed. The basic idea of damage mechanics is to

E-mail address: cvolokh@tx.technion.ac.il.

0022-5096/$ - see front matter © 2007 Elsevier Ltd. All rights reserved.
doi:10.1016/j.jmps.2007.02.012

introduce a damage parameter, scalar or tensor, which describes the degradation of material properties during mechanical loading (Kachanov, 1958, 1986; Krajcinovic, 1996; Skrzypek and Ganczarski, 1999; Lemaitre and Desmorat, 2005). The damage parameter is an internal variable though its possible interpretation as a volumetric density of voids or microcracks is reasonable. The magnitude of the damage parameter is constrained by (a) a damage evolution equation and (b) a critical threshold condition similar to the plasticity theories. Theoretically, the approach of damage mechanics is very flexible and allows reflecting the physical processes triggering macroscopic damage at small length scales. Practically, the experimental calibration of damage theories is far from trivial. It is difficult to measure the damage parameter directly. The experimental calibration should be implicit and it should include both the damage evolution equation and the damage criticality condition. Because of these difficulties, it seems reasonable to look for alternative theories that present the bulk material failure in more feasible ways than the traditional damage theories. Softening hyperelasticity is a possible candidate for a simple description of material failure.

The roots of the softening hyperelasticity approach can be traced to atomistic analysis of fracture relating material debonding to atomic separation. Gao and Klein (1998) and Klein and Gao (1998) and, more recently, Volokh and Gao (2005) and Volokh and Ramesh (2006) showed how to mix the atomistic and continuum material descriptions in order to simulate the failure process—the virtual internal bond (VIB) method. They applied the Cauchy–Born rule linking microscopic and macroscopic length scales to empirical potentials, which include a possibility of the full atomic separation. The continuum-atomistic linkage led to the formulation of macroscopic strain energy potentials allowing for the stress/strain softening and strain localization. The continuum-atomistic method is very effective at small length scales where purely atomistic analysis becomes computationally intensive. This approach found applications in bio- and nano-mechanics concerning the problems of bone fracture (Gao et al., 2003; Ji and Gao, 2004) and strength of carbon nanotubes (Zhang et al., 2004; Volokh and Ramesh, 2006). Unfortunately, the direct use of the continuum-atomistic method in macroscopic damage problems is not very feasible because its computer implementation includes a numerically involved procedure of the averaging of the interatomic potentials over a representative volume.

As a macroscopic alternative to the continuum-atomistic method, a phenomenological softening hyperelasticity approach for modeling materials failure has been considered by Volokh (2004, 2007) for the isotropic Hookean solid. An expression of the strain energy was found that enforces strain softening controlled by material constants. Unfortunately, the strain energy expression considered in the cited works is material-specific and it is not readily extended to other materials. *In the present work, we lift the softening hyperelasticity approach to a level of generality and introduce a universal formula for the treatment of material failure*. Now any hyperelastic material model can be enhanced with softening automatically. The softening is controlled by constant Φ of the critical failure energy indicating the maximum strain energy that the infinitesimal material volume can sustain without failure. This constant can be interpreted as the material 'toughness' analogously to the critical energy release rate in the classical fracture mechanics (Bazant and Planas, 1998; Broberg, 1999; Hertzberg, 1989; Kanninen and Popelaar, 1973; Knott, 1985). Despite the analogy, the difference between the classical fracture mechanics and softening hyperelasticity should not be missed. The classical fracture mechanics introduces the length-dependence in the failure calculations because of the introduction of the surface

energy. The length-dependence may lead to physically meaningless results as will be emphasized later (Section 5). The softening hyperelasticity approach does not introduce the surface energy and the length-dependence in harmony with the physical intuition. We examine the proposed approach on a variety of the boundary value problems with a variety of material models.

The paper is organized as follows. The basic equations of nonlinear continuum mechanics are reviewed in Section 2. The general concept of softening hyperelasticity is formalized in Section 3. The simple shear and uniaxial tension examples that can be used for the experimental calibration of the critical strain energy are considered in Section 4. The spherically symmetric problems of cavitation and balloon inflation are analyzed in Sections 5 and 6 accordingly. The arterial failure calculations are given in Section 7. The motivation for the introduction of the concept of the critical failure energy based on the atomistic considerations is presented in Section 8. Discussion of the obtained results and a possible finite element implementation of softening hyperelasticity appears in Section 9.

2. Basic equations

We consider the classical formulation of nonlinear continuum mechanics (Truesdell and Noll, 2003) according to which a generic material particle of body Ω occupying position $\mathbf{X}$ at the reference state moves to position $\mathbf{x}(\mathbf{X})$ at the current state. The deformation of the particle is defined by the tensor of deformation gradient $\mathbf{F}=\partial\mathbf{x}/\partial\mathbf{X}$.

The equilibrium equation in Ω and boundary conditions on $\partial\Omega$ are set in the Eulerian form as follows:

$$\operatorname{div}\boldsymbol{\sigma}=\mathbf{0}, \tag{2.1}$$

$$\mathbf{x}=\bar{\mathbf{x}} \quad \text{or} \quad \boldsymbol{\sigma}\mathbf{n}=\bar{\mathbf{t}}, \tag{2.2}$$

where 'div' operator is with respect to current coordinates $\mathbf{x}$; $\boldsymbol{\sigma}$ is the Cauchy stress tensor; $\mathbf{t}$ is traction per unit area of the current surface with the unit outward normal $\mathbf{n}$; and the barred quantities are prescribed.

Alternatively, the equilibrium equation and boundary conditions can be set in the Lagrangian form as follows

$$\operatorname{Div}\mathbf{P}=\mathbf{0}, \tag{2.3}$$

$$\mathbf{x}=\bar{\mathbf{x}} \quad \text{or} \quad \mathbf{P}\mathbf{n}_0=\bar{\mathbf{t}}_0, \tag{2.4}$$

where 'Div' operator is with respect to referential coordinates $\mathbf{X}$; $\mathbf{P}$ is the 1st Piola–Kirchhoff stress tensor; $\mathbf{t}_0$ is traction per unit area of the reference surface with the unit outward normal $\mathbf{n}_0$; and the barred quantities are prescribed.

The Eulerian and Lagrangian quantities are related as follows:

$$\mathbf{n}=\mathbf{F}^{-\mathrm{T}}\mathbf{n}_0|\mathbf{F}^{-\mathrm{T}}\mathbf{n}_0|^{-1}, \tag{2.5}$$

$$\boldsymbol{\sigma}=J^{-1}\mathbf{P}\mathbf{F}^{\mathrm{T}}, \tag{2.6}$$

$$\mathbf{t}=\mathbf{t}_0J^{-1}|\mathbf{F}^{-\mathrm{T}}\mathbf{n}_0|^{-1}, \tag{2.7}$$

$$J=\det\mathbf{F}. \tag{2.8}$$

We consider a purely mechanical theory for a hyperelastic material described by the strain energy, $\psi(\mathbf{C})$, which depends on the right Cauchy–Green deformation tensor

$$\mathbf{C} = \mathbf{F}^{\mathrm{T}}\mathbf{F}. \tag{2.9}$$

The constitutive equation can be written in the general form

$$\mathbf{P} = 2\mathbf{F}\frac{\partial \psi}{\partial \mathbf{C}}, \tag{2.10}$$

or

$$\boldsymbol{\sigma} = 2J^{-1}\mathbf{F}\frac{\partial \psi}{\partial \mathbf{C}}\mathbf{F}^{\mathrm{T}}. \tag{2.11}$$

Eqs. (2.1), (2.2), (2.11) or (2.3), (2.4), (2.10) set the boundary value problem of hyperelasticity in Eulerian or Lagrangian formulation accordingly.

3. Hyperelastic material with softening

Traditionally, the strain energy of hyperelastic materials is defined as

$$\psi = W, \tag{3.1}$$

where W is used for the strain energy of the *intact* material.

For example, the isotropic Hookean model presenting the behavior of many engineering materials under small deformations is described by

$$W = \lambda(\mathbf{E} : \mathbf{1})^2/2 + \mu\mathbf{E} : \mathbf{E}, \tag{3.2}$$

where λ and μ are the Lame material constants and

$$\mathbf{E} = (\mathbf{C} - \mathbf{1})/2 \approx (\mathbf{H} + \mathbf{H}^{\mathrm{T}})/2 \tag{3.3}$$

is the Green strain; $\mathbf{1}$ is the second-order identity tensor and $\mathbf{H} = \partial\mathbf{u}/\partial\mathbf{X}$ is the displacement, $\mathbf{u} = \mathbf{x} - \mathbf{X}$, gradient. The second approximate equality in (3.3) is valid for small deformations.

Another example is the Mooney–Rivlin isotropic model presenting rubber-like materials

$$W = \alpha(I_1 - 3)/2 + \beta(I_2 - 3)/2, \tag{3.4}$$

where α and β are the material constants and

$$I_1 = \mathbf{C} : \mathbf{1}, \tag{3.5}$$

$$I_2 = (I_1^2 - \mathbf{C}^2 : \mathbf{1})/2 \tag{3.6}$$

are the first and the second principal invariants of $\mathbf{C}$. Mooney–Rivlin materials are usually assumed incompressible, $\det \mathbf{F} = 1 = \det \mathbf{C}$, which leads to the appearance of an undefined pressure-like term, $-p\mathbf{1}$, in the expression of the true stress. This term, p, is the Lagrange multiplier, which enforces the geometric incompressibility constraint.

The Neo-Hookean material is obtained for $\beta = 0$ in (3.4).

Final example is the Fung-type model of soft biological tissues

$$W = \gamma(\mathrm{e}^{Q(\mathbf{C})} - 1), \tag{3.7}$$

where γ is a material constant and Q is a function of $\mathbf{C}$. Biological materials are usually assumed incompressible because their response to hydrostatic stresses is much stronger

than their response to shearing. In this sense, the soft tissues resemble fluids. Actually, many soft tissues are saturated by fluids what partially justifies the incompressibility assumption. It seems, however, that the applicability of the incompressibility assumption essentially depends on the specific loading and deformation of the material under consideration (Volokh, 2006a).

The mentioned models and their modifications present a wide variety of engineering and biological materials. It is important to realize that the traditional constitutive models target intact materials predominantly. It is reasonable in this case to assume that the mathematically correct model should provide the existence of the solution of the corresponding boundary value problem and the stability of the numerical algorithm implementing this solution. Such a desire gave rise, for example, to the famous Ball (1977) results on polyconvexity of the strain energy functions.

Simplistically, the intact material models can be characterized as follows:

$$\|\mathbf{C}\| \to \infty \Rightarrow \psi \to \infty, \tag{3.8}$$

where $\|\dots\|$ is a tensorial norm. In other words, the increasing strain increases the accumulated energy and *the possible energy increase is unlimited*.

Evidently, the consideration of only intact materials is restrictive and no real material can sustain large enough strains. The latter means that the energy increase should be limited by a critical value

$$\|\mathbf{C}\| \to \infty \Rightarrow \psi = \Phi = \text{constant}, \tag{3.9}$$

where Φ can be called the *material failure energy*.

By analogy with the classical fracture mechanics where only one constant of material toughness (or the critical energy release rate) is introduced to describe failure we assume that Φ is the only constant characterizing the material failure properties. Despite the analogy, we should strongly emphasize the difference between the classical fracture mechanics and the softening hyperelasticity approach advocated in the present work. The former approach introduces the length-dependence in the failure calculations because of the introduction of the surface energy. The length-dependence may lead to physically meaningless results as will be shown later. The latter approach does not introduce the surface energy and, consequently, the length-dependence in harmony with the physical intuition as will be discussed later.

There is a variety of possibilities to formulate the strain energy obeying condition (3.9). Our desire, however, is to enrich the already existing models, which describe intact behavior of materials reasonably well, with the failure condition. Such a desire can be formalized as follows:

$$\|\mathbf{C}\| \to \infty \Rightarrow \psi(W(\mathbf{C})) = \Phi = \text{constant}. \tag{3.10}$$

In other words, we are looking for a strain energy expression, ψ, which is a function of the strain energy of an intact material, W. A possible solution to this problem is

$$\psi(W) = \Phi - \Phi \exp(-W/\Phi), \tag{3.11}$$

where

$$\psi(W = 0) = 0 \tag{3.12}$$

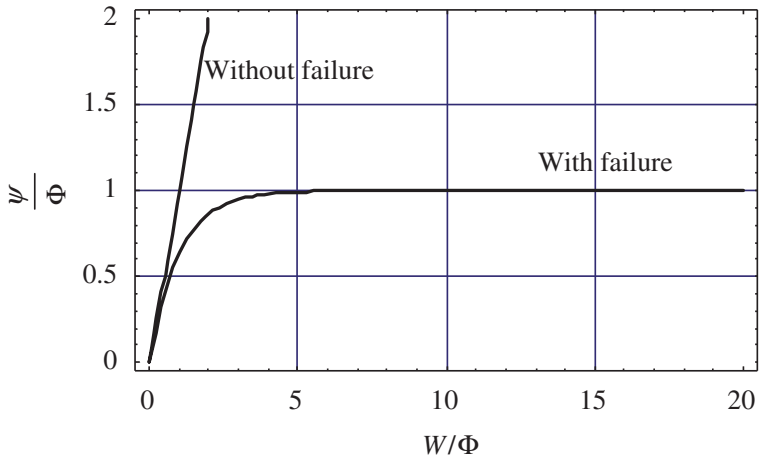

Fig. 1. Strain energy with and without failure.

and

$$\psi(W=\infty)=\Phi. \tag{3.13}$$

We notice that in the case of the intact material behavior

$$\frac{W}{\Phi}\ll 1, \tag{3.14}$$

the power series expansion of (3.11) reads

$$\psi(W)\approx W \tag{3.15}$$

preserving the features of the intact material (Fig. 1).

Substituting (3.11) in (2.10), (2.11) we have accordingly

$$\mathbf{P}=2\mathbf{F}\frac{\partial W}{\partial \mathbf{C}}\exp(-W/\Phi), \tag{3.16}$$

$$\boldsymbol{\sigma}=2J^{-1}\mathbf{F}\frac{\partial W}{\partial \mathbf{C}}\mathbf{F}^{\mathrm{T}}\exp(-W/\Phi). \tag{3.17}$$

Thus, the exponential multiplier enforces material softening and the models based on (3.16), (3.17) can be called *hyperelasticity with softening* or, simpler, *softening hyperelasticity*. Our subsequent analysis of examples aims at elaborating on the presented formulation of softening hyperelasticity.

4. Calibration: simple shear and uniaxial tension

We consider simple shear and uniaxial tension problems for brittle and soft materials accordingly in this section. Their solutions can be used for the experimental calibration of the models.

4.1. Simple shear of isotropic Hookean material

We start with the simple shear of an isotropic Hookean material under small deformations. In this case, we have

$$\mathbf{E} = \gamma(\mathbf{e}_1 \otimes \mathbf{e}_2 + \mathbf{e}_2 \otimes \mathbf{e}_1), \tag{4.1}$$

$$\boldsymbol{\sigma} = \tau(\mathbf{e}_1 \otimes \mathbf{e}_2 + \mathbf{e}_2 \otimes \mathbf{e}_1), \tag{4.2}$$

and the Hooke law with softening

$$\boldsymbol{\sigma} \cong \frac{\partial W}{\partial \mathbf{E}} \exp(-W/\Phi) = (2\mu\mathbf{E} + \lambda(\mathbf{E} : \mathbf{1})\mathbf{1}) \exp(-W/\Phi) \tag{4.3}$$

reduces to

$$\tau = 2\mu\gamma \exp(-2(\lambda + \mu)\gamma^2/\Phi), \tag{4.4}$$

where $\mathbf{e}_i$ is the Cartesian basis.

The shape of this curve appears in Fig. 2. Qualitatively, this means that the magnitude of the shear stress increases with the shear strain, reaches a maximum, and then approaches zero with increasing failure. The local maximum of the curve is at point $\gamma_{\max} = \pm\sqrt{\Phi/(\lambda + \mu)}/2$. Assume, for example, that the maximum experimental shear for the given material is $\gamma_{\max} = 10^{-3}$. Then, we have $(\lambda + \mu)/\Phi = 2.5 \times 10^5$ and $\tau/\mu = 2\gamma \exp(-5 \times 10^5\gamma^2)$—Fig. 2.

4.2. Uniaxial tension of Neo-Hookean material

Next, we consider the uniaxial tension of the Neo-Hookean material with softening. This material is a particular case of the Mooney–Rivlin class of materials and it is described as follows:

$$W(I_1) = \frac{\alpha}{2}(I_1 - 3), \tag{4.5}$$

$$\boldsymbol{\sigma} = -p\mathbf{1} + 2W_1\mathbf{B} \exp(-W/\Phi), \tag{4.6}$$

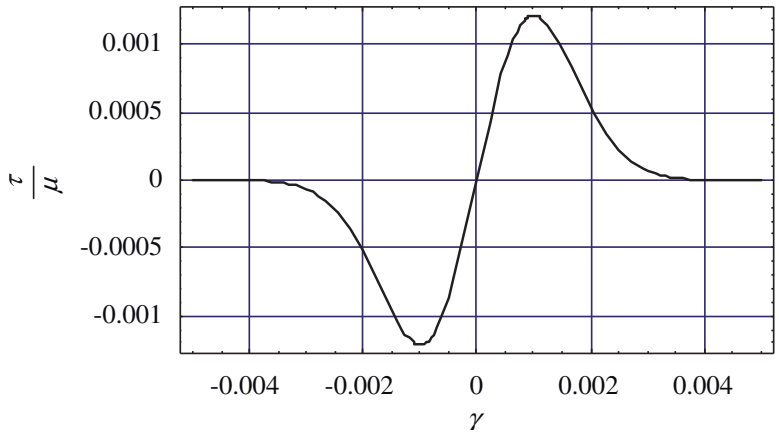

Fig. 2. Simple shear with softening.

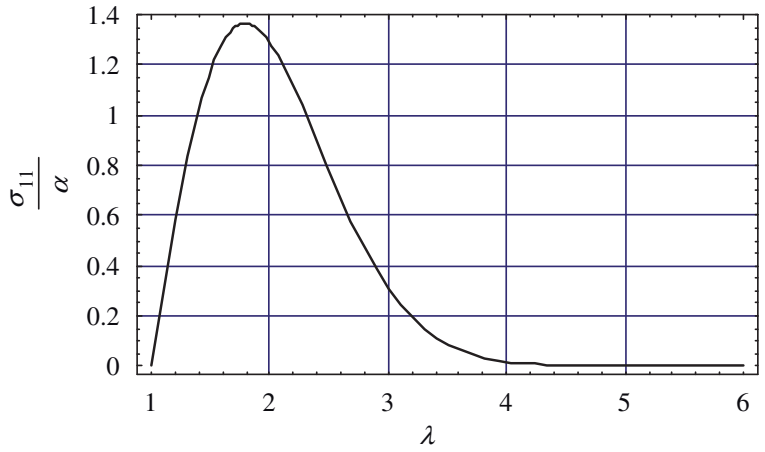

Fig. 3. Uniaxial tension of the Neo-Hookean material with softening.

where

$$\mathbf{B} = \mathbf{F}\mathbf{F}^{\mathrm{T}}, \tag{4.7}$$

$$W_i \equiv \partial W/\partial I_i. \tag{4.8}$$

In the case of uniaxial tension the deformation is

$$x_1 = \lambda X_1; \quad x_2 = \lambda^{-1/2} X_2; \quad x_3 = \lambda^{-1/2} X_3, \tag{4.9}$$

$$\mathbf{B} = \lambda^2 \mathbf{e}_1 \otimes \mathbf{e}_1 + \lambda^{-1}(\mathbf{e}_2 \otimes \mathbf{e}_2 + \mathbf{e}_3 \otimes \mathbf{e}_3), \tag{4.10}$$

where λ designates stretch.

Based on (4.6) we find[1]

$$\begin{aligned} \sigma_{11} &= 2(\lambda^2 - \lambda^{-1}) W_1 \exp(-W/\Phi) \\ &= \alpha(\lambda^2 - \lambda^{-1}) \exp\{-\alpha(\lambda^2 + 2\lambda^{-1} - 3)/(2\Phi)\}. \end{aligned} \tag{4.11}$$

The stress–stretch curve described by (4.11) is shown in Fig. 3. The maximum point on the curve corresponding to the softening material indicates the onset of the material failure/rupture. After the stretch reaches the magnitude of $\sim$1.8 ($\alpha = \Phi$) no stable solution of the statical problem exists. The uniaxial tension test can be used for the calibration of the material failure constant Φ. Indeed, measuring the critical stretch one can fit the load–stretch curve and find the constant.

4.3. Tension of bio-fiber

Finally, we consider the tension test of a biological fiber described in the following strain energy function and the constitutive law (Holzapfel et al., 2000):

$$W(J) = \frac{k_1}{2k_2}(\exp(k_2(J-1)^2) - 1), \tag{4.12}$$

$$\boldsymbol{\sigma} = 2\frac{\partial W}{\partial J}\,\mathbf{m} \otimes \mathbf{m} \exp(-W/\Phi), \tag{4.13}$$

[1]This is an extension of the celebrated Rivlin's (1948) solution to the case with softening.

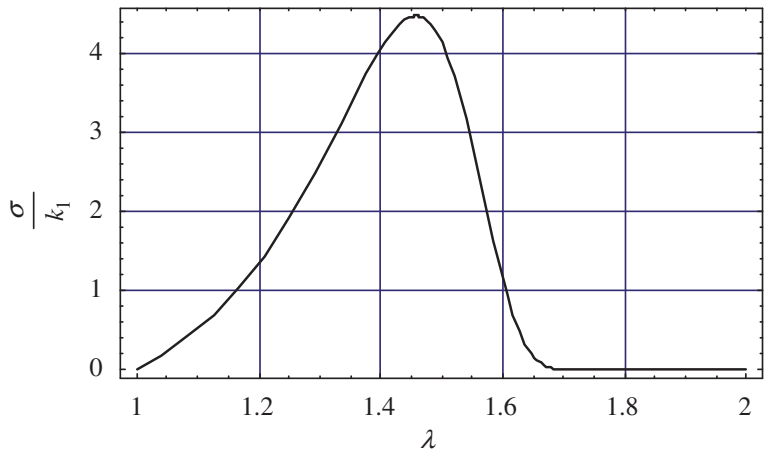

Fig. 4. Tension of a bio-fiber with softening.

where

$$\mathbf{m} = \mathbf{F}\mathbf{M}, \tag{4.14}$$

$$J = \mathbf{m} \cdot \mathbf{m}, \tag{4.15}$$

and $\mathbf{M}$ ($|\mathbf{M}| = 1$) is the initial fiber direction.

In the case of tension of an individual fiber we have $\mathbf{m} = \lambda \mathbf{M}$ and $J = \lambda^2$, consequently, the stress–stretch curve is given by

$$\sigma \equiv \frac{\mathbf{m} \cdot \boldsymbol{\sigma}\mathbf{m}}{\mathbf{m} \cdot \mathbf{m}} = 2\lambda^2 \frac{\partial W}{\partial J} \exp(-W/\Phi). \tag{4.16}$$

Fig. 4 presents the stress–stretch curve of a bio-fiber with constants $k_1 = 2.3632\,\text{kPa}$ and $k_2 = 0.8392$. The magnitudes are experimentally calibrated for the medial arterial fibers (see Section 7). We also assumed $\Phi = k_1$ in Fig. 4. As in the previous example, the experimental calibration of a specific fiber can be made.

5. Cavitation problem

In this section, we consider the cavitation problem for the Hookean and Neo-Hookean materials with softening.

5.1. Cavitation in isotropic Hookean solid

Let us start with the centrally symmetric deformation of a spherical void of radius a in a Hookean sphere of radius b. In this case small displacements we will not make difference between the referential and current configurations. The displacement and strains take the following form in spherical coordinates $\{r, \theta, \omega\}$:

$$\mathbf{u} = u(r)\,\mathbf{g}_r, \tag{5.1}$$

$$\mathbf{E} = E_{rr}\mathbf{g}_r \otimes \mathbf{g}_r + E_{\theta\theta}\mathbf{g}_\theta \otimes \mathbf{g}_\theta + E_{\omega\omega}\mathbf{g}_\omega \otimes \mathbf{g}_\omega, \tag{5.2}$$

$$E_{rr} = \frac{\partial u}{\partial r}; \quad E_{\theta\theta} = \frac{u}{r}; \quad E_{\omega\omega} = \frac{u}{r}, \tag{5.3}$$

where

$$\begin{cases} \mathbf{g}_r = (\sin\theta\cos\omega, \sin\theta\sin\omega, \cos\theta)^{\mathrm{T}}, \\ \mathbf{g}_\theta = (\cos\theta\cos\omega, \cos\theta\sin\omega, -\sin\theta)^{\mathrm{T}}, \\ \mathbf{g}_\omega = (-\sin\omega, \cos\omega, 0)^{\mathrm{T}}. \end{cases} \tag{5.4}$$

The stress tensor takes the form

$$\boldsymbol{\sigma} = \sigma_{rr}\mathbf{g}_r \otimes \mathbf{g}_r + \sigma_{\theta\theta}\mathbf{g}_\theta \otimes \mathbf{g}_\theta + \sigma_{\omega\omega}\mathbf{g}_\omega \otimes \mathbf{g}_\omega, \tag{5.5}$$

$$\begin{cases} \sigma_{rr} = (2\mu E_{rr} + \lambda \mathbf{E} : \mathbf{1})\exp(-W/\Phi), \\ \sigma_{\theta\theta} = (2\mu E_{\theta\theta} + \lambda \mathbf{E} : \mathbf{1})\exp(-W/\Phi), \\ \sigma_{\omega\omega} = (2\mu E_{\omega\omega} + \lambda \mathbf{E} : \mathbf{1})\exp(-W/\Phi), \end{cases} \tag{5.6}$$

$$W = \lambda(E_{rr} + E_{\theta\theta} + E_{\omega\omega})^2/2 + \mu(E_{rr}^2 + E_{\theta\theta}^2 + E_{\omega\omega}^2), \tag{5.7}$$

and the equilibrium equation reduces to

$$\frac{\partial\sigma_{rr}}{\partial r} + 2\frac{\sigma_{rr} - \sigma_{\theta\theta}}{r} = 0. \tag{5.8}$$

Two boundary conditions are imposed on it

$$\begin{cases} \sigma_{rr}(r = a) = 0, \\ \sigma_{rr}(r = b) = p. \end{cases} \tag{5.9}$$

Substituting (5.3) and (5.6) in (5.8) and (5.9) we obtain a nonlinear two-point boundary value problem in terms of radial displacement u.

Numerical solution of the described problems is generated by using the shooting method with a displacement control. According to it, we, first, make the initial guess for displacement $u^{(0)}$ at the void surface $r = a$. Second, we calculate $(\partial u/\partial r)^{(0)}$ at the void surface from condition $(5.9)_1$. Third, we solve the initial value problem with given $u^{(0)}$ and $(\partial u/\partial r)^{(0)}$. The latter step is accomplished by using the 'NDSolve' numerical integrator of Mathematica for the solution of the initial value problem. Three mentioned steps are repeated iteratively unless the normal stress at the outer surface $r = b$ converges to the given magnitude p and condition $(5.9)_2$ is obeyed.

The curve presenting the critical pressure versus the changing void size curve is shown in Fig. 5 for $\mu/\Phi = 15 \times 10^5/11$ and $\mu/\lambda = 6/5$. The curve does not change for $b/a > b/a > 10$, i.e. *the critical tension is independent of the void size.*

By way of contrast, we present the critical hydrostatic tension obtained by using the Griffith energy approach (Volokh, 2007)

$$p_c = \sqrt{\frac{2EG_c}{3(1-\nu)a}}, \tag{5.10}$$

where E is the Young modulus; ν is the Poisson ratio; $a \ll b$; and the critical energy release rate G_c is a material constant. Thus, the critical tension is inversely proportional to the square root of the void radius. *The critical tension can increase unlimitedly with the radius decrease.* The latter conclusion is physically meaningless, of course.

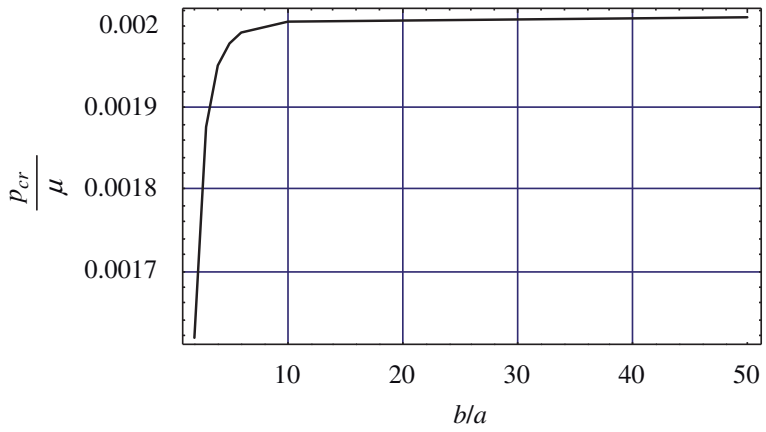

Fig. 5. Critical hydrostatic tension versus the void size for the Hookean material with softening.

5.2. Cavitation in isotropic Neo-Hookean solid

Next, let us consider cavitation in the Neo-Hookean softening material. In this case, we assume

$$r = r(R), \quad \theta = \Theta, \quad \omega = \Omega, \tag{5.11}$$

where a point occupying position (R, Θ, Ω) in the initial configuration is moving to position (r, θ, ω) in the current configuration. Then the deformation gradient takes the form

$$\mathbf{F} = (\partial r/\partial R)\,\mathbf{g}_r \otimes \mathbf{G}_R + (r/R)\,\mathbf{g}_\theta \otimes \mathbf{G}_\Theta + (r/R)\mathbf{g}_\omega \otimes \mathbf{G}_\Omega, \tag{5.12}$$

where the current base vectors were defined in (5.4) and the referential base vectors are

$$\begin{cases} \mathbf{G}_R = (\sin\Theta\cos\Omega, \sin\Theta\sin\Omega, \cos\Theta)^{\mathrm{T}}, \\ \mathbf{G}_\Theta = (\cos\Theta\cos\Omega, \cos\Theta\sin\Omega, -\sin\Theta)^{\mathrm{T}}, \\ \mathbf{G}_\Omega = (-\sin\Omega, \cos\Omega, 0)^{\mathrm{T}}. \end{cases} \tag{5.13}$$

It is worth mentioning that material incompressibility implies

$$\frac{\partial r}{\partial R} = \frac{R^2}{r^2}. \tag{5.14}$$

Designating the radii of the void A and a before and after the deformation accordingly, we can integrate (5.14) and get

$$r^3 - a^3 = R^3 - A^3. \tag{5.15}$$

In view of (5.12) and (5.14), the left Cauchy–Green deformation tensor takes the form

$$\mathbf{B} = (R/r)^4\,\mathbf{g}_r \otimes \mathbf{g}_r + (r/R)^2\,\mathbf{g}_\theta \otimes \mathbf{g}_\theta + (r/R)^2\mathbf{g}_\omega \otimes \mathbf{g}_\omega, \tag{5.16}$$

and the constitutive equations (4.5) and (4.6) take the following form:

$$\begin{cases} \sigma_{rr} = -p + \alpha(R/r)^4 \exp\left\{-\dfrac{\alpha}{2}(I_1 - 3)/\Phi\right\}, \\ \sigma_{\theta\theta} = \sigma_{\omega\omega} = -p + \alpha(r/R)^2 \exp\left\{-\dfrac{\alpha}{2}(I_1 - 3)/\Phi\right\}. \end{cases} \tag{5.17}$$

In the case under consideration, we have only one scalar Eulerian equation of equilibrium

$$\frac{\partial \sigma_{rr}}{\partial r} + 2\frac{\sigma_{rr} - \sigma_{\theta\theta}}{r} = 0. \tag{5.18}$$

This equation is completed with two boundary conditions

$$\begin{cases} \sigma_{rr}(r = a) = 0, \\ \sigma_{rr}(r = b) = g. \end{cases} \tag{5.19}$$

The traction-free condition is set at the edge of the void. The hydrostatic tension g is imposed at the remote boundary, whose radius changes from B to b during deformation.

Integrating (5.18) with account of (5.19) we have

$$g = 2\int_a^b \frac{\sigma_{\theta\theta} - \sigma_{rr}}{r}\,\mathrm{d}r = 2\alpha\int_a^b (r^2/R^2 - R^4/r^4)\exp\left\{-\frac{\alpha}{2}(I_1 - 3)/\Phi\right\}\frac{\mathrm{d}r}{r}, \tag{5.20}$$

where $I_1 = R^4/r^4 + 2r^2/R^2$ and $R^2 = (r^3 - a^3 + A^3)^{2/3}$.

We introduce new variables to reformulate (5.20) in the dimensionless form

$$\bar{g} = \frac{g}{\alpha}; \quad \bar{r} = \frac{r}{A}; \quad \bar{R} = \frac{R}{A}; \quad \bar{a} = \frac{a}{A}; \quad \bar{b} = \frac{b}{A}. \tag{5.21}$$

Substituting (40) in (39) we have

$$\bar{g} = 2\int_{\bar{a}}^{\bar{b}} (\bar{r}^2/\bar{R}^2 - \bar{R}^4/\bar{r}^4)\exp\left\{-\frac{\alpha}{2\Phi}(\bar{R}^4/\bar{r}^4 + 2\bar{r}^2/\bar{R}^2 - 3)\right\}\frac{\mathrm{d}\bar{r}}{\bar{r}}, \tag{5.22}$$

where $\bar{R}^2 = (\bar{r}^3 - \bar{a}^3 + 1)^{2/3}$ and we choose $\Phi = \alpha$. We track the hydrostatic tension, $\bar{g}$, versus void expansion, $\bar{a}$, curve—Fig. 6. It is remarkable that the curve does not change for varying $\bar{b}$ starting from $\bar{b} > 40\bar{a}$. *This observation can be interpreted as the independence of the critical tension on the size of the void for small voids*. Evidently, dynamic analysis of failure propagation is necessary when the tension reaches the critical value. The classical Neo-Hookean material without softening exhibits the asymptotic convergence to the tension magnitude $g/\alpha = 5/2$ as expected.

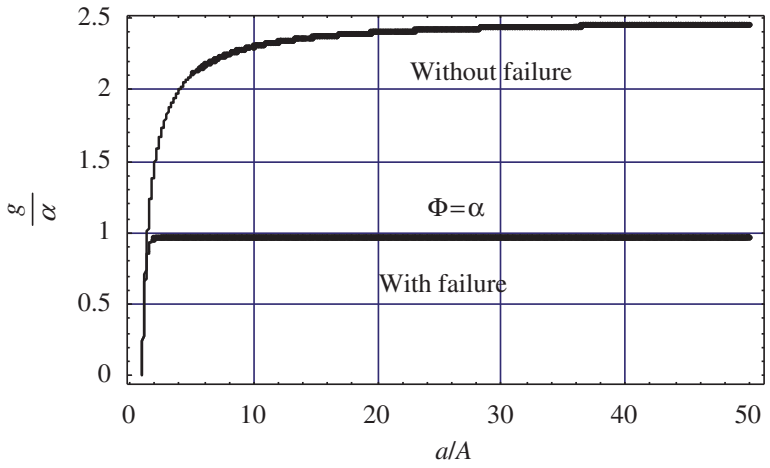

Fig. 6. Hydrostatic tension versus void radius for the Neo-Hookean material with and without softening.

6. Balloon rupture

In this section, we examine the balloon inflation problem for various materials.

6.1. General formulae

Restricting attention to spherically symmetric deformations of incompressible materials we will use the general pressure–stretch solution as it appears in Beatty (1987) and can be traced back to Green and Zerna (1954) and Green and Adkins (1960):

$$p(\lambda) = \frac{4h}{\lambda R}(1-\lambda^{-6})(\psi_1 + \lambda^2\psi_2), \tag{6.1}$$

where $\psi_i = \partial\psi/\partial I_i$; $h \ll R$ is the thickness of the balloon; R is its initial radius; $\lambda = r/R$ is the stretch where r is the current radius and the principal invariants are

$$I_1 = 2\lambda^2 + \lambda^{-4}, \tag{6.2}$$

$$I_2 = (2\lambda^2 + \lambda^{-4})^2/2 - (2\lambda^4 + \lambda^{-8})/2. \tag{6.3}$$

In the case of material with softening, we can rewrite (6.1) as follows:

$$p(\lambda) = \frac{4h}{\lambda R}(1-\lambda^{-6})(W_1 + \lambda^2 W_2)\exp(-W/\Phi). \tag{6.4}$$

To ignore softening one sets $\Phi \to \infty$ and the exponential multiplier disappears.

6.2. Inflation of Mooney–Rivlin balloon

We start by examining the Mooney–Rivlin material $W = \alpha(I_1 - 3)/2 + \beta(I_2 - 3)/2$. In this case (6.4) takes the form

$$p(\lambda) = (2h\alpha/R)\lambda^{-1}(1-\lambda^{-6})(1+\gamma\lambda^2)\exp(-\alpha(I_1 - 3 + \gamma(I_2 - 3))/2\Phi). \tag{6.5}$$

Fig. 7 presents two curves described by (6.5) and generated for $\gamma = \beta/\alpha = 0.055$ with, $\Phi/\alpha = 2500$, and without, $\Phi/\alpha = \infty$, softening. It is remarkable that both curves exhibit the first limit point, which is observed in the balloon inflation experiments in the intact

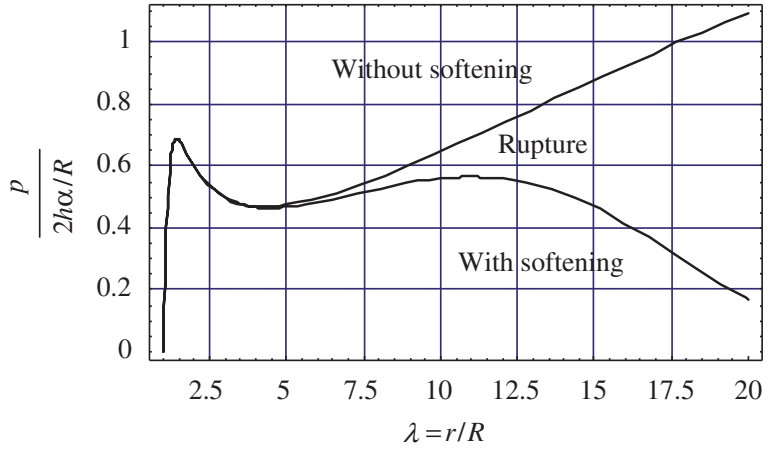

Fig. 7. Inflation of the balloon made of the Mooney–Rivlin material.

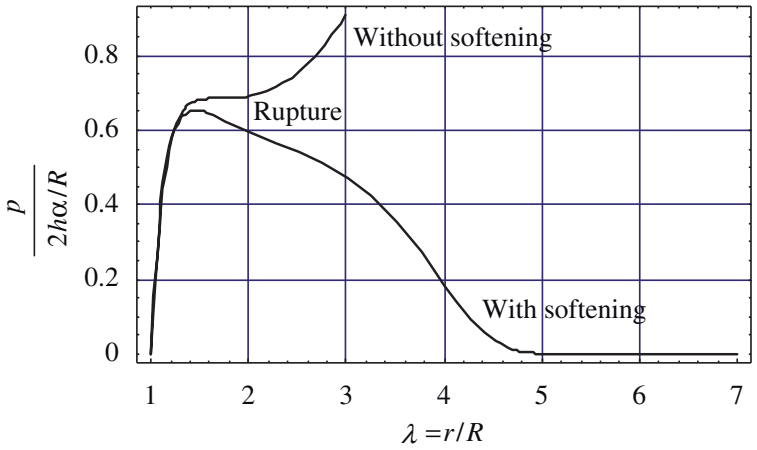

Fig. 8. Inflation of the balloon made of the Fung-type biomaterial.

rubber-like materials, while the second limit point indicating rupture can be captured by the model with softening only.

6.3. *Inflation of Fung-type (biomaterial) balloon*

We turn now to a biological tissue defined by the Fung-type strain energy

$$W = \frac{\alpha}{2\beta}\{\exp(\beta(I_1 - 3)) - 1\}, \tag{6.6}$$

where α and β are material constants.

In this case, (6.4) takes the form

$$p(\lambda) = (2\alpha h/R)\lambda^{-1}(1 - \lambda^{-6})\exp(\beta(I_1 - 3))\exp(-W/\Phi). \tag{6.7}$$

Fig. 8 presents two curves described by (6.7) and generated for $\beta = 0.067$ with, $\Phi/\alpha = 20$, and without, $\Phi/\alpha = \infty$, softening. Evidently, the biomaterial without softening is not capable of capturing rupture.

7. Arterial failure

In this section, we use the softening hyperelasticity approach to study arterial failure. Histological analysis of the arterial wall (Humphrey, 2002) reveals that the artery comprises three layers—intima, media, and adventitia. While the mechanical role of intima is minor, media and adventitia contribute to the arterial strength. Both media and adventitia are anisotropic composite materials where the cellular matrix is reinforced with a net of oriented elastin and collagen microfibers. There are a number of constitutive theories presenting passive behavior of *intact* arteries which include material anisotropy (Vaishnav et al., 1973; Fung et al., 1979; von Maltzahn et al., 1981; Chuong and Fung, 1983; Tözeren, 1984; Demiray, 1991; Humphrey, 1995; Wuyts et al., 1995; Delfino et al., 1997; Simon et al., 1998a, b). We choose the latest theory proposed by Holzapfel et al. (2000) to account for the bi-layer structure of the artery where both adventitia and media are fiber-reinforced composites.

We ignore the residual stresses, which develop during artery growth because of the following two reasons. First, we assume that such stresses do not affect the failure

predictions targeted below. Second, the existing approach to estimating residual stresses based on the ring-cutting experiments is somewhat open to discussion (Rachev and Greenwald, 2003; Volokh, 2006b).

Holzapfel et al. (2000) suggest writing the constitutive equations *for adventitia or media* in the following form:

$$\boldsymbol{\sigma} = \boldsymbol{\sigma}^{M} + \boldsymbol{\sigma}^{F_1} + \boldsymbol{\sigma}^{F_2}, \tag{7.1}$$

$$\boldsymbol{\sigma}^{M} = -p\mathbf{1} + 2W_1^{M}\mathbf{B}, \tag{7.2}$$

$$\boldsymbol{\sigma}^{F_1} = 2W_1^{F_1}\mathbf{m}_1 \otimes \mathbf{m}_1, \tag{7.3}$$

$$\boldsymbol{\sigma}^{F_2} = 2W_2^{F_2}\mathbf{m}_2 \otimes \mathbf{m}_2. \tag{7.4}$$

Here the Cauchy stress tensor is decomposed into $\boldsymbol{\sigma}^{M}$ representing the layer matrix and $\boldsymbol{\sigma}^{F_1}$ and $\boldsymbol{\sigma}^{F_2}$ representing two families of fibers; $W^{M}(I_1)$ is the strain energy of the matrix; vectors $\mathbf{m}_i = \mathbf{F}\mathbf{M}_i$ designate 'pushed forward' initial fiber units $\mathbf{M}_i$ ($|\mathbf{M}_i| = 1$); $W^{F_i}(J_i)$ is the strain energy of the stretching fibers: $J_i = \mathbf{m}_i \cdot \mathbf{m}_i$; and $W_1^{M} \equiv \partial W^{M}/\partial I_1$; $W_i^{F_i} \equiv \partial W^{F_i}/\partial J_i$.

The matrix material is Neo-Hookean:

$$W^{M}(I_1) = \frac{\alpha}{2}(I_1 - 3), \tag{7.5}$$

while the fibers are described by the exponential stored energy

$$W^{F_i}(J_i) = \frac{k_1}{2k_2}\{\exp(k_2(J_i - 1)^2) - 1\}, \tag{7.6}$$

where α, k_1, k_2 are the material constants.

Enforcing softening in accordance with (3.11) we replace (7.5) and (7.6) by the following formulae accordingly:

$$\psi^{M} = \Phi^{M} - \Phi^{M}\exp(-W^{M}/\Phi^{M}), \tag{7.7}$$

$$\psi^{F_i} = \Phi^{F_i} - \Phi^{F_i}\exp(-W^{F_i}/\Phi^{F_i}), \tag{7.8}$$

where Φ^{M}, Φ^{F_i} are material failure constants equal to the limit strain energies.

We consider a radial inflation of an artery as a symmetric deformation of a cylinder under the plane strain conditions

$$r = r(R), \quad \theta = \Theta, \quad z = Z, \tag{7.9}$$

where a point occupying position (R, Θ, Z) in the initial configuration is moving to position (r, θ, z) in the current configuration. Then, the deformation gradient takes the form

$$\mathbf{F} = (\partial r/\partial R)\,\mathbf{g}_r \otimes \mathbf{G}_R + (r/R)\,\mathbf{g}_\theta \otimes \mathbf{G}_\Theta + \mathbf{g}_z \otimes \mathbf{G}_Z, \tag{7.10}$$

where the orthonormal bases in cylindrical coordinates at the reference and current configurations take the following forms accordingly:

$$\mathbf{G}_R = (\cos\Theta, \sin\Theta, 0)^{\mathrm{T}}; \quad \mathbf{G}_\Theta = (-\sin\Theta, \cos\Theta, 0)^{\mathrm{T}}; \quad \mathbf{G}_Z = (0, 0, 1)^{\mathrm{T}}, \tag{7.11}$$

$$\mathbf{g}_r = (\cos\theta, \sin\theta, 0)^{\mathrm{T}}; \quad \mathbf{g}_\theta = (-\sin\theta, \cos\theta, 0)^{\mathrm{T}}; \quad \mathbf{g}_z = (0, 0, 1)^{\mathrm{T}}. \tag{7.12}$$

Incompressibility condition implies for (7.10)

$$\det \mathbf{F} = \frac{\partial r}{\partial R}\frac{r}{R} = 1 \tag{7.13}$$

or

$$\frac{\partial r}{\partial R} = \frac{R}{r}. \tag{7.14}$$

Designating the internal radii of the artery A and a before and after the deformation accordingly, we can integrate (7.14) and get

$$r^2 - a^2 = R^2 - A^2. \tag{7.15}$$

In view of (7.10) and (7.14), the left Cauchy–Green deformation tensor takes form

$$\mathbf{B} = \mathbf{F}\mathbf{F}^{\mathrm{T}} = (R/r)^2\,\mathbf{g}_r \otimes \mathbf{g}_r + (r/R)^2\,\mathbf{g}_\theta \otimes \mathbf{g}_\theta + \mathbf{g}_z \otimes \mathbf{g}_z. \tag{7.16}$$

The fiber kinematics is described by

$$\mathbf{m}_1 = \mathbf{F}\mathbf{M}_1 = (r\cos\beta/R)\,\mathbf{g}_\theta + (\sin\beta)\mathbf{g}_z, \tag{7.17}$$

$$\mathbf{m}_2 = \mathbf{F}\mathbf{M}_2 = (r\cos\beta/R)\,\mathbf{g}_\theta - (\sin\beta)\mathbf{g}_z, \tag{7.18}$$

where the initial fiber directions are $\mathbf{M}_1 = \cos\beta\,\mathbf{G}_\Theta + \sin\beta\,\mathbf{G}_Z$ and $\mathbf{M}_2 = \cos\beta\,\mathbf{G}_\Theta - \sin\beta\,\mathbf{G}_Z$. Here β is the angle between the fibers and the circumferential direction of the artery.

Gathering all terms with the help of (7.1)–(7.8) and (7.16)–(7.18) we get the nontrivial components of the Cauchy stress:

$$\begin{cases} \sigma_{rr} = -p + 2\psi_1^M (R/r)^2, \\ \sigma_{\theta\theta} = -p + 2\psi_1^M (r/R)^2 + 2(\psi_1^{F_1} + \psi_2^{F_2})(r/R)^2\cos^2\beta, \\ \sigma_{zz} = -p + 2\psi_1^M + 2(\psi_1^{F_1} + \psi_2^{F_2})\sin^2\beta \end{cases} \tag{7.19}$$

and strain invariants

$$\begin{cases} I_1 = (r/R)^2 + (R/r)^2 + 1, \\ J_1 = J_2 = (r/R)^2\cos^2\beta + \sin^2\beta. \end{cases} \tag{7.20}$$

There is only one nontrivial equilibrium equation

$$\frac{\partial \sigma_{rr}}{\partial r} + \frac{\sigma_{rr} - \sigma_{\theta\theta}}{r} = 0, \tag{7.21}$$

and the traction boundary conditions are

$$\begin{cases} \sigma_{rr}(r = a) = -g, \\ \sigma_{rr}(r = b) = 0, \end{cases} \tag{7.22}$$

where b is the outer radius of the artery after the deformation, which was equal to B before the deformation.

We integrate equilibrium equation (7.21) over the wall thickness with account of boundary conditions (7.22) and get

$$g(a) = -\int_a^{b(a)} (\sigma_{rr} - \sigma_{\theta\theta}) \frac{\mathrm{d}r}{r}$$
$$= -\int_a^{b(a)} (2\psi_1^M (R/r)^2 - 2\psi_1^M (r/R)^2 - 4\psi_1^{F_1} (r/R)^2 \cos^2\beta) \frac{\mathrm{d}r}{r}, \tag{7.23}$$

where $b(a) = \sqrt{a^2 + B^2 - A^2}$ because of the incompressibility condition and $\psi_1^{F_1} = \psi_2^{F_2}$.

Eq. (7.23) presents the pressure–radius (g–a) relationship, which we examine for various material constants. Before doing that, however, we introduce dimensionless variables as follows:

$$\bar{g} = \frac{g}{\alpha}; \quad \bar{r} = \frac{r}{A}; \quad \bar{R} = \frac{R}{A}; \quad \bar{a} = \frac{a}{A}; \quad \bar{b} = \frac{b}{A}. \tag{7.24}$$

Now (7.23) takes the form

$$\bar{g}(\bar{a}) = -\int_{\bar{a}}^{\bar{b}(\bar{a})} (2(\bar{R}/\bar{r})^2 \bar{\psi}_1^M - 2(\bar{r}/\bar{R})^2 \bar{\psi}_1^M - 4(\bar{r}/\bar{R})^2 \bar{\psi}_1^{F_1} \cos^2\beta) \frac{\mathrm{d}\bar{r}}{\bar{r}}, \tag{7.25}$$

where

$$\bar{b}(\bar{a}) = \sqrt{\bar{a}^2 + (B/A)^2 - 1}, \tag{7.26}$$

$$\bar{\psi}_1^M = \frac{1}{2} \exp\left\{ -\frac{\alpha}{2\Phi^M} (I_1 - 3) \right\}, \tag{7.27}$$

$$\bar{\psi}_1^{F_1} = \frac{k_1}{\alpha \Phi^{F_1}} (J_1 - 1) \exp(k_2 (J_1 - 1)^2) \exp\left\{ -\frac{k_1}{2k_2 \Phi^{F_1}} [\exp(k_2 (J_1 - 1)^2) - 1] \right\}, \tag{7.28}$$

$$I_1 = (\bar{r}/\bar{R})^2 + (\bar{R}/\bar{r})^2 + 1, \tag{7.29}$$

$$J_1 = (\bar{r}/\bar{R})^2 \cos^2\beta + \sin^2\beta, \tag{7.30}$$

$$\bar{R}^2 = (\bar{r}^2 - \bar{a}^2) + 1. \tag{7.31}$$

It should not be missed that material constants change from media to adventitia and, thus, the integral in (7.25) is additively split into computations in two integrals for the media and adventitia accordingly.

The purpose of numerical simulations is twofold. First, we aim at clarifying the relative importance of matrix and fibers within the media layer[2] of the arterial wall. Second, we examine the comparative contribution of the adventitia and the media in the overall arterial strength.

As a 'ground state' of material constants, which will vary in calculations, we choose the parameters reported by Holzapfel et al. (2000) for the media: $c_M = 3.0\,\mathrm{kPa}$, $k_{1M} = 2.3632\,\mathrm{kPa}$, $k_{2M} = 0.8392$, $A = 0.7\,\mathrm{mm}$, $B_M = 0.96\,\mathrm{mm}$, $\beta_M = \pi/6$; and for the adventitia: $c_A = 0.3\,\mathrm{kPa}$, $k_{1A} = 0.562\,\mathrm{kPa}$, $k_{2A} = 0.7112$, $A_A = B_M$ (the media–adventitia

[2]We choose the media because it is stiffer than the adventitia.

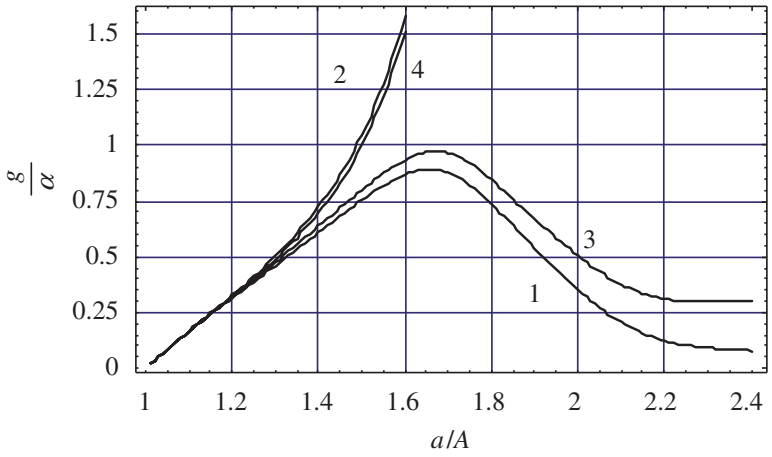

Fig. 9. Pressure–displacement curve for the 'ground state' of the inflating media: matrix and fibers with softening, 1; matrix and fibers without softening, 2; fibers with and matrix without softening, 3; matrix with and fibers without softening, 4.

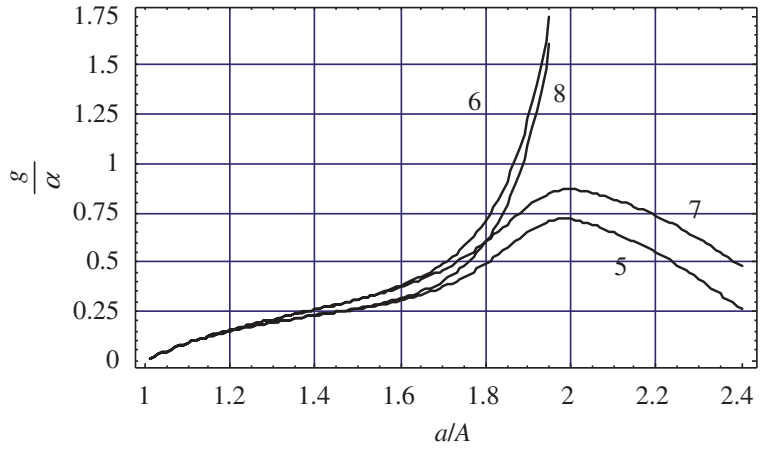

Fig. 10. Pressure–displacement curve for the decreased fiber stiffness: matrix and fibers with softening, 5; matrix and fibers without softening, 6; fibers with and matrix without softening, 7; matrix with and fibers without softening, 8.

interface), $B = 1.09\,\text{mm}$, $\beta_A = \pi/3$. These parameters were fitted to the experimental data of Chuong and Fung (1983) for a carotid artery of a rabbit. We complete the softening hyperelastic model with material constants controlling failure of the media and the adventitia accordingly: $\Phi_M^M = \alpha_M$, $\Phi_M^{F_1} = k_{1M}$ and $\Phi_A^M = \alpha_A$, $\Phi_A^{F_1} = k_{1A}$.

The pressure–radius curve #1 in Fig. 9 presents the media failure for the ground state. In this case the softening is allowed for both matrix and fibers. The media without softening, i.e. $\Phi_M^M = \infty$ and $\Phi_M^{F_1} = \infty$, is presented by curve #2. The case where the matrix does not soften while the fibers do, i.e. $\Phi_M^M = \infty$, is presented by curve #3 and the case where the fibers do not soften while the matrix does, i.e. $\Phi_M^{F_1} = \infty$, is presented by curve #4. It is readily observed in Fig. 9 that *the overall strength is controlled by the strength of the fibers*. Indeed, when the fibers soften the media softens and when the fibers do not the media does not.

Further, Figs. 10 and 11, we examine the effect of the 10 times decrease $k_{1M} = 0.23632\,\text{kPa}$ and the 10 times increase $k_{1M} = 23.632\,\text{kPa}$ of the fiber stiffness accordingly. We repeat all previous calculations for the entirely softening media, curves #5 and #9, the

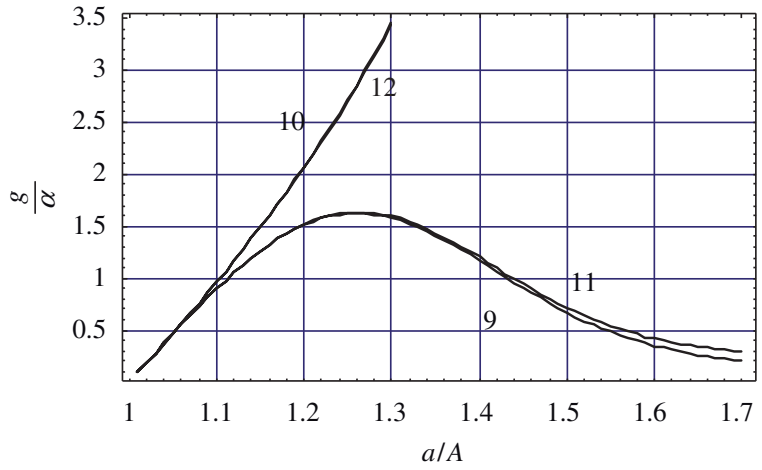

Fig. 11. Pressure–displacement curve for the increased fiber stiffness: matrix and fibers with softening, 9; matrix and fibers without softening, 10; fibers with and matrix without softening, 11; matrix with and fibers without softening, 12.

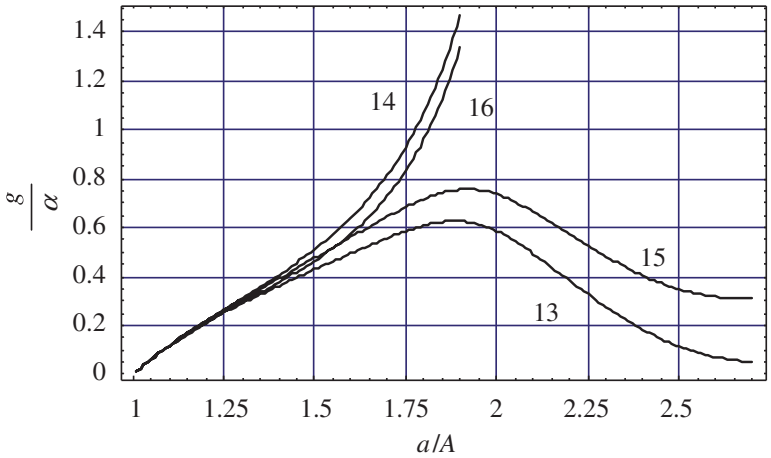

Fig. 12. Pressure–displacement curve for the increased fiber angle: matrix and fibers with softening, 13; matrix and fibers without softening, 14; fibers with and matrix without softening, 15; matrix with and fibers without softening, 16.

media without softening, curves #6 and #10, the case where the matrix does not soften while the fibers do, curves #7 and #11, and the case where the fibers do not soften while the matrix does, curves #8 and #12. Though the quantitative changes are evident as compared to Fig. 9 the qualitative conclusion remains the same: *the overall strength is controlled by the strength of the fibers*.

Then, Figs. 12 and 13, we examine the effect of the increase $\beta_M = \pi/4$ of the fiber angle and the increase $\Phi_M^M = 10\alpha_M$ of the matrix failure constant accordingly. We repeat all previous calculations for the entirely softening media, curves #13 and #17, the media without softening, curves #14 and #18, the case where the matrix does not soften while the fibers do, curves #15 and #19, and the case where the fibers do not soften while the matrix does, curves #16 and #20. Though the quantitative changes are again evident as compared to Fig. 9 the qualitative conclusion remains the same again: *the overall strength is controlled by the strength of the fibers*.

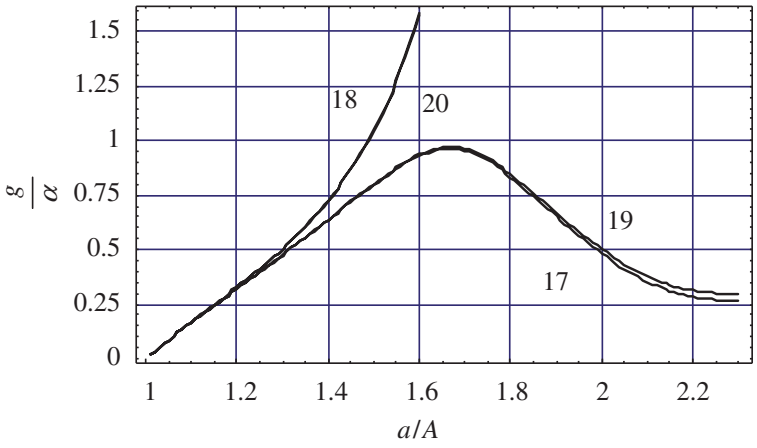

Fig. 13. Pressure–displacement curve for the increased matrix failure constant: matrix and fibers with softening, 17; matrix and fibers without softening, 18; fibers with and matrix without softening, 19; matrix with and fibers without softening, 20.

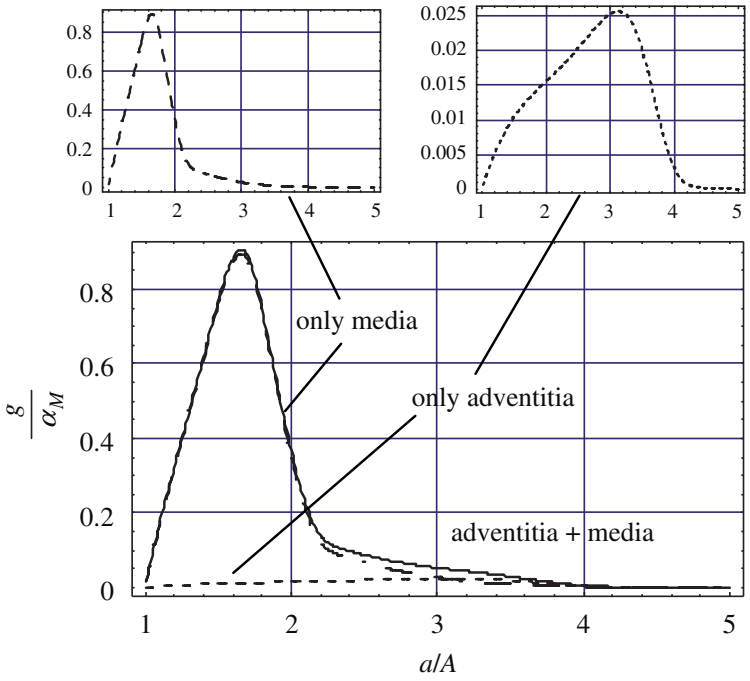

Fig. 14. Pressure–displacement curve for the 'ground state' of the bi-layer arterial wall model.

At this point, our first task, the examination of the relative contribution of the matrix and fibers to the overall layer strength, is accomplished. We turn to the second task—examination of the relative contribution of the media and the adventitia to the overall layer strength.

The pressure–radius curve for the bi-layer arterial model including the media and the adventitia is presented in Fig. 14 for the 'ground state' of material constants described above. The figure also includes the separate contributions of the media and adventitia shown by the dashed lines. The considered set of material constants led to the domination of the media strength. This situation can change when the adventitia fibers enjoy the fiber constant $\Phi_A^{F_1} = 10k_{1A}$ as shown in Fig. 15. In this case, the adventitia strength is pronounced though the media strength is still higher.

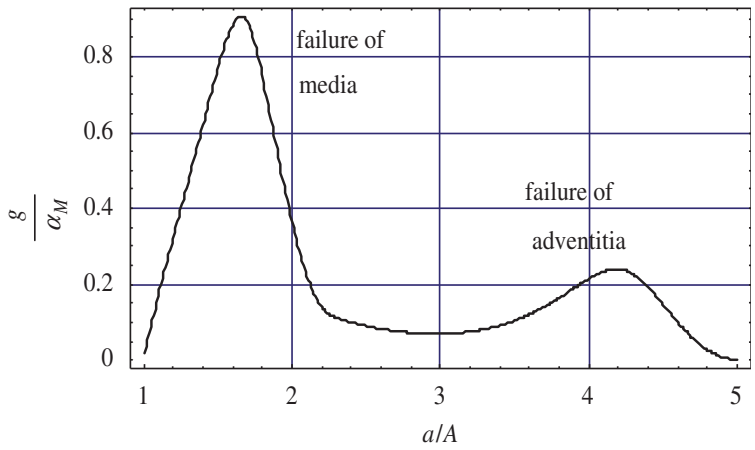

Fig. 15. Pressure–displacement curve for the increased failure constant of the adventitia fibers of the bi-layer arterial wall model.

8. Critical failure energy: continuum-atomistic link

This section aims at justifying the assumption of the existence of the critical failure energy, Φ. We consider the continuum-atomistic link for materials that can be described by the Lennard-Jones or Morse interatomic potentials, for example, and we show how the macroscopic parameter Φ can be calculated.

Consider a solid body comprising microparticles, for example atoms, placed at $\mathbf{r}_i$ in the 3D space. Generally, the volumetric density of the total potential energy of the body is a function of the particle positions: $E(\mathbf{r}_1, \mathbf{r}_2, \ldots, \mathbf{r}_N)$, where N is the number of particles. More specifically, the potential energy density, i.e. the strain energy, can be written with account of the two-particle interactions as follows:

$$\psi = \frac{E}{2V} = \frac{1}{2V} \sum_{i,j} U(r_{ij}), \tag{8.1}$$

$$r_{ij} = |\mathbf{r}_{ij}| = |\mathbf{r}_i - \mathbf{r}_j|, \tag{8.2}$$

where V is the volume occupied by the system.

According to the Cauchy–Born rule, originally applied to the crystal elasticity, the current $\mathbf{r}_{ij}$ and initial (reference) $\mathbf{R}_{ij} = \mathbf{R}_i - \mathbf{R}_j$ relative positions of the same two particles can be related by the deformation gradient, Fig. 16,

$$\mathbf{r}_{ij} = \mathbf{F}\mathbf{R}_{ij}. \tag{8.3}$$

It is assumed here that the deformation is locally homogeneous.

Substituting (8.3) in (8.1) and (8.2) yields

$$\psi = \frac{1}{2V} \sum_{i,j} U(r_{ij}) = \psi(\mathbf{C}). \tag{8.4}$$

Direct application of (8.4) to analysis of material behavior can be difficult because of the large amount of microparticles. Gao and Klein (1998) and Klein and Gao (1998, 2000)

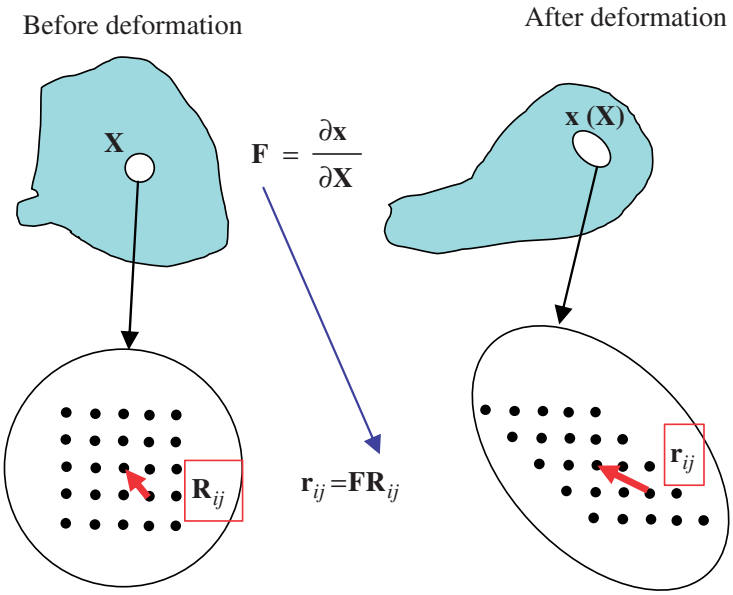

Fig. 16. Cauchy–Born rule.

considered the following averaging procedure:

$$\psi = \langle U(l) \rangle \equiv \frac{1}{V_0} \int_{V_0^*} U(l) D_V \, \mathrm{d}V. \tag{8.5}$$

Here V_0 is the reference representative volume; l is the current virtual bond length; $U(l)$ is the bonding potential; D_V is the volumetric bond density function; and V_0^* is the integration volume defined by the range of influence of U.

Introducing new notation it is possible to write

$$l = r_{ij} = L\sqrt{\boldsymbol{\xi}} \cdot \mathbf{C}\boldsymbol{\xi} = L|\mathbf{F}\boldsymbol{\xi}|, \tag{8.6}$$

$$L = R_{ij} = |\mathbf{R}_i - \mathbf{R}_j|, \tag{8.7}$$

$$\boldsymbol{\xi} = (\mathbf{R}_i - \mathbf{R}_j)/L. \tag{8.8}$$

We start with considering the critical failure energy predictions based on the Lennard-Jones potential

$$V(l) = 4\varepsilon((\sigma/l)^{12} - (\sigma/l)^6), \tag{8.9}$$

where ε and σ are the bond energy and length constants—Fig. 17. The minimum of $V = -\varepsilon$ is reached at the equilibrium bond length $l = \sqrt[6]{2}\sigma$ where no forces are acting between the atoms.

In view of the continuum-atomistic link discussed above, we shift the energy expression (8.9) by ε to provide the zero minimum energy of the referential equilibrium state of the bond deformation:

$$U(l) = 4\varepsilon((\sigma/l)^{12} - (\sigma/l)^6) + \varepsilon. \tag{8.10}$$

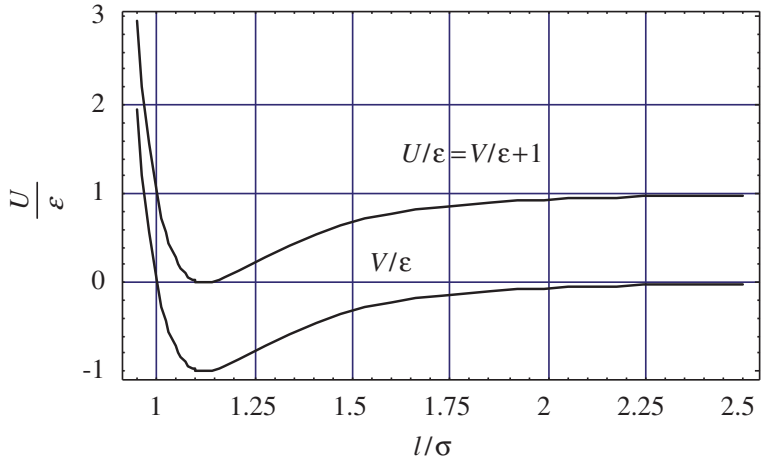

Fig. 17. Lennard-Jones potential.

Then (8.5) takes the form

$$\psi(\mathbf{C}) = \frac{1}{V_0}\int_{V_0^*} (4(\sigma/L\sqrt{\boldsymbol{\xi}\cdot\mathbf{C}\boldsymbol{\xi}})^{12} - 4(\sigma/L\sqrt{\boldsymbol{\xi}\cdot\mathbf{C}\boldsymbol{\xi}})^{6} + 1)\varepsilon D_V \,\mathrm{d}V, \tag{8.11}$$

where (8.6) and (8.10) have been used.

It is important to emphasize that the equilibrium bond length in a lattice is not necessarily equivalent to the equilibrium bond length in a pair of atoms: $L = \sqrt[6]{2}\sigma$. The calculation of the equilibrium bond length in a lattice can generally be nontrivial and require a numerical minimization procedure. Moreover, the interatomic forces may differ from zero for pairs of atoms though the average force can be assumed zero.

We can define the critical energy value from (8.11) by using (3.10) as follows:

$$\Phi = \psi(\|\mathbf{C}\| \to \infty) = \frac{1}{V_0}\int_{V_0^*} \varepsilon D_V \,\mathrm{d}V, \tag{8.12}$$

where

$$\|\mathbf{C}\| = \sqrt{\boldsymbol{\xi}\cdot\mathbf{C}\boldsymbol{\xi}} \tag{8.13}$$

for any $\boldsymbol{\xi}$.

Now we consider the critical failure energy predictions based on the Morse potential

$$V(l) = \varepsilon(\mathrm{e}^{-2\beta(l-L)} - 2\mathrm{e}^{-\beta(l-L)}), \tag{8.14}$$

where ε and L are the bond energy and equilibrium length accordingly, while β is a constant having the inverse length dimension—Fig. 18. The minimum of $V = -\varepsilon$ is reached at the equilibrium bond length $l = L$ where no forces are acting between the atoms.

In view of the continuum-atomistic link discussed above, we shift the energy expression (8.14) by ε to provide the zero minimum energy of the referential equilibrium state of the bond deformation:

$$U(l) = \varepsilon(\mathrm{e}^{-2\beta(l-L)} - 2\mathrm{e}^{-\beta(l-L)} + 1). \tag{8.15}$$

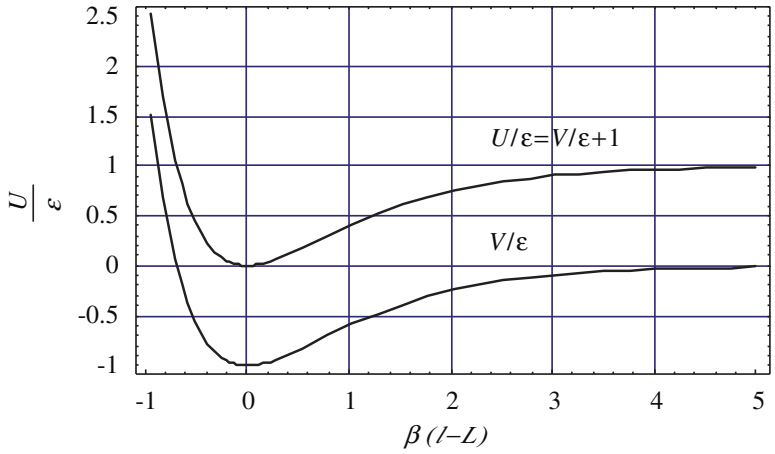

Fig. 18. Morse potential.

Then (8.5) takes the form

$$\psi(\mathbf{C}) = \frac{1}{V_0}\int_{V_0^*}\{\exp[2\beta L(1-\sqrt{\boldsymbol{\xi}\cdot\mathbf{C}\boldsymbol{\xi}})] - 2\exp[\beta L(1-\sqrt{\boldsymbol{\xi}\cdot\mathbf{C}\boldsymbol{\xi}})] + 1\}\varepsilon D_V\,\mathrm{d}V, \tag{8.16}$$

where (8.6) and (8.15) have been used.

Again, we emphasize that the equilibrium bond length in a lattice is not necessarily equivalent to the equilibrium bond length in a pair of atoms.

We can define the critical failure energy value from (8.16) by using (3.10) as follows:

$$\Phi = \psi(\|\mathbf{C}\| \to \infty) = \frac{1}{V_0}\int_{V_0^*}\varepsilon D_V\,\mathrm{d}V, \tag{8.17}$$

where $\|\mathbf{C}\| = \sqrt{\boldsymbol{\xi}\cdot\mathbf{C}\boldsymbol{\xi}}$ for any $\boldsymbol{\xi}$.

9. Discussion

In the present work, we proposed a new approach of softening hyperelasticity for modeling materials failure. We assumed the existence of the maximum constant value of strain energy, Φ, associated with the onset of material failure. This constant represents the material 'toughness'. We proposed a simple and *universal* formula, (3.11), to account for possible failure of *any* hyperelastic material. It is important that the formula preserves all features of behavior of intact materials unless the strain energy approaches the energy limit, Φ. We examined the softening hyperelasticity approach considering a variety of materials and boundary value problems.

It was shown, first, that simple shear and uniaxial tension experiments can be used for the failure calibration of brittle Hookean and soft hyperelastic materials.

Then, we considered cavitation (void instability) under the hydrostatic tension. In the case of the isotropic Hookean material, we found that the critical tension did not depend on the void size for small voids. This result is physically reasonable if we assume that the failure process develops due to the stresses/strains at the edge of the void. Such stresses/strains do not depend on the void size and, consequently, the critical tension should not depend on the void size. The situation, however, is strikingly different if one uses the

Griffith energy method for the prediction of the critical tension. In the latter case, the critical tension depends on the inverse square root of the void radius and tends to infinity when the radius decreases. Evidently, the Griffith analysis brings physically meaningless results. The reason for that is the length-dependence of the Griffith approach, which contradicts the length-independence of the classical continuum mechanics. Indeed, Griffith introduces the surface energy into consideration and, as a result, he sets a characteristic length, say, the volume energy over the surface energy for example. Separation of the failure condition from stress analysis is the main disease of the Griffith approach. An interested reader is referred to Volokh (2007) for a detailed discussion of the issue.

The study of the cavitation in the softening Neo-Hookean material reveals the existence of the critical tension where the dynamic failure propagation starts. This is in contrast to the intact Neo-Hookean material where the critical tension does not exist. We should note that the asymptotic value of the maximum tension existing for the intact Neo-Hookean material could not be considered as a material failure indicator, as sometimes assumed, because the material behavior is always stable.

Our examination of the balloon inflation problem further reveals the capacity of the proposed framework to capture material failure. The intact biological material considered in the present work did not exhibit any instability while its model with softening had the instability point indicating the rupture onset. In this regard, the example of the inflating Mooney–Rivlin balloon (Fig. 7) is remarkably instructive. The intact Mooney–Rivlin material captures the phenomenon of the balloon softening presented by the first limit point. It is unable, however, to capture rupture. The Mooney–Rivlin material enhanced with softening exhibits two limit points where the second one corresponds to rupture.

We also examined the strength of the arterial wall. The wall included two layers of media and adventitia. Every layer comprised a cellular matrix described by the Neo-Hookean isotropic material with softening and two families of fibers described by the exponential stored energy function with softening. We considered the axisymmetric inflation of the wall under internal pressure and it was found that the fiber strength dominates the overall arterial strength. Such qualitative conclusion has an immediate experimental implication: it is necessary to calibrate the mechanical models of individual fibers in order to predict the global arterial strength. It was also found that the relative contribution of media and adventitia to the arterial strength depends on the relative strength of the fibers belonging in media and adventitia.

Finally, we tracked the continuum-atomistic link allowing for the derivation of the parameter of the critical failure energy, Φ. We showed how to derive it for the materials that can be described by the Lennard-Jones or Morse potentials, for example.

Bearing in mind limitations of the present study, we should note that the softening hyperelasticity approach targets brittle materials and soft hyperelastic materials predominantly. The presented formulation is unable to handle failure of ductile materials exhibiting essential plastic deformations before failure. Neither the proposed approach is relevant to the micro-scale problems showing the pronounced length-dependence.

Considering further limitations of the present study, we should emphasize that the softening hyperelasticity approach was used in the analytically tractable problems and, consequently, the deformation modes were restrictive. To relax these restrictions general finite element methods should be used within the softening hyperelasticity framework. Two numerical problems concerning the finite element implementation should be addressed. First, it is necessary to introduce the energy dissipation in the finite element model in order

to preclude from the material healing. This can be done, for example, by decreasing the material constants within a finite element by a few orders of magnitude after the element energy reaches the critical value of the volumetric failure work. In other words, the damaged material should have new and low magnitudes of the material constants. The second issue is related with the necessity to regularize the ill-posed numerical problem where the loss of ellipticity/hyperbolicity of the governing equations with softening can lead to the pathological mesh-sensitivity (Crisfield, 1997; Belytschko et al., 2000; de Borst, 2001). The regularization procedure should introduce a characteristic length in the calculation precluding the mesh sensitivity. Three following approaches are considered in the literature to regularize the numerical problem of the FE-mesh sensitivity. The first approach suggests replacing the classical continuum formulation with a generalized continuum formulation—higher-order, gradient, or non-local theories (de Borst and van der Giessen, 1998). The generalized continuum formulations introduce material length parameters, which control the strain localization processes. The only shortcoming of the generalized continuum formulations is the need to give a clear physical interpretation to the necessary additional boundary conditions. The second approach goes back to the work of Hillerborg et al. (1976). The basic idea of this approach is to introduce a characteristic material length directly in the FE model bypassing the PDE formulation. This approach was adapted by ABAQUS for the analysis of concrete structures. The third approach to the treatment of mesh sensitivity can be called dynamic regularization. The basic idea of this approach is to introduce the characteristic length in the problem implicitly through the rate dependence of the constitutive or balance equations. Needleman (1988), for example, observed that rate-dependence of the material regularizes the ill-posed numerical problem. He notes, however, that whether or not the introduced implicit length-scale is relevant depends on the particular circumstances. Another sort of regularization was reported by Zhang et al. (2002), who added the viscous forces to the momentum balance equations within the framework of the continuum-atomistic method. They observed in simulations that the artificial dumping suppressed the mesh sensitivity. These results are promising and they can be applied for the regularization of the failure evolution problem within the framework of the softening hyperelasticity theory proposed in the present work.

References

Ball, J.M., 1977. Convexity conditions and existence theorems in non-linear elasticity. Arch. Ration. Mech. Anal. 63, 337–403.

Bazant, Z.P., Planas, J., 1998. Fracture and Size Effect of Concrete and Other Quasibrittle Materials. CRC Press, Boca Raton.

Beatty, M.F., 1987. Topics in finite elasticity: hyperelasticity of rubber, elastomers, and biological tissues—with examples. Appl. Mech. Rev. 40, 1699–1734.

Belytschko, T., Liu, W.K., Moran, B., 2000. Nonlinear Finite Elements for Continua and Structures. Wiley, New York.

de Borst, R., 2001. Some recent issues in computational failure mechanics. Int. J. Numer. Methods Eng. 52, 63–95.

de Borst, R., van der Giessen, E., 1998. Material Instabilities in Solids. Wiley, Chichester.

Broberg, K.B., 1999. Cracks and Fracture. Academic Press, London.

Chuong, C.J., Fung, Y.C., 1983. Three-dimensional stress distribution in arteries. J. Biomech. Eng. 105, 268–274.

Crisfield, M.A., 1997. Non-linear Finite Element Analysis of Solids and Structures, vol. 2. Wiley, Chichester.

Delfino, A., Stergiopulos, N., Moore, J.E., Meister, J.-J., 1997. Residual strain effects on the stress field in a thick wall finite element model of the human carotid bifurcation. J. Biomech. 30, 777–786.

Demiray, H., 1991. A layered cylindrical shell model for an aorta. Int. J. Eng. Sci. 29, 47–54.
Fung, Y.C., Fronek, K., Patitucci, P., 1979. Pseudoelasticity of arteries and the choice of its mathematical expression. Am. J. Physiol. 237, H620–H631.
Gao, H., Klein, P., 1998. Numerical simulation of crack growth in an isotropic solid with randomized internal cohesive bonds. J. Mech. Phys. Solids 46, 187–218.
Gao, H., Ji, B., Jager, I.L., Arzt, E., Fratzl, P., 2003. Materials become insensitive to flaws at nanoscale: lessons from nature. Proc. Nat. Acad. Sci. 100, 5597–5600.
Green, A.E., Adkins, J.E., 1960. Large Elastic Deformations. Oxford University Press, London.
Green, A.E., Zerna, W., 1954. Theoretical Elasticity. Oxford University Press, London.
Hertzberg, R.W., 1989. Deformation and Fracture of Engineering Materials, third ed. Wiley, New York.
Hillerborg, A., Modeer, M., Peterson, P.E., 1976. Analysis of crack growth in concrete by means of fracture mechanics and finite elements. Cem. Concr. Res. 6, 773–782.
Holzapfel, G.A., Gasser, T.C., Ogden, R.W., 2000. A new constitutive framework for arterial wall mechanics and a comparative study of material models. J. Elasticity 61, 1–48.
Humphrey, J.D., 1995. Mechanics of arterial wall: review and directions. Crit. Rev. Biomed. Eng. 23, 1–162.
Humphrey, J.D., 2002. Cardiovascular Solid Mechanics: Cells, Tissues, and Organs. Springer, New York.
Ji, B., Gao, H., 2004. A study of fracture mechanisms in biological nano-composites via the virtual internal bond model. Mater. Sci. Eng. A366, 96–103.
Kachanov, L.M., 1958. Time of the rupture process under creep conditions. Izvestiia Akademii Nauk SSSR, Otdelenie Teckhnicheskikh Nauk 8, 26–31.
Kachanov, L.M., 1986. Introduction to Continuum Damage Mechanics. Martinus Nijhoff Dordrecht, The Netherlands.
Kanninen, M.F., Popelaar, C., 1973. Fundamentals of Fracture Mechanics. Butterworth, London.
Klein, P., Gao, H., 1998. Crack nucleation and growth as strain localization in a virtual-bond continuum. Eng. Fract. Mech. 61, 21–48.
Klein, P., Gao, H., 2000. Study of crack dynamics using the virtual internal bond method. In: Multiscale Deformation and Fracture in Materials and Structures. Kluwer, Dodrecht, pp. 275–309.
Knott, J.F., 1985. Advanced Fracture Mechanics. Oxford University Press.
Krajcinovic, D., 1996. Damage Mechanics. Elsevier, North Holland Series in Applied Mathematics and Mechanics.
Lemaitre, J., Desmorat, R., 2005. Engineering Damage Mechanics: Ductile, Creep, Fatigue and Brittle failures. Springer, Berlin.
von Maltzahn, W.-W., Besdo, D., Wiemer, W., 1981. Elastic properties of arteries: a nonlinear two-layer cylindrical model. J. Biomech. 14, 389–397.
Needleman, A., 1988. Material rate dependence and mesh sensitivity in localization problems. Comput. Methods Appl. Mech. Eng. 67, 69–85.
Rachev, A., Greenwald, S.E., 2003. Residual stresses in conduit arteries. J. Biomech. 36, 661–670.
Rivlin, R.S., 1948. Large elastic deformations of isotropic materials. IV. Further developments of the general theory. Philos. Trans. R. Soc. London A241, 379–397.
Simon, B.R., Kaufmann, M.V., McAfee, M.A., Baldwin, A.L., 1998a. Porohyperelastic finite element analysis of large arteries using ABAQUS. J. Biomech. Eng. 120, 296–298.
Simon, B.R., Kaufmann, M.V., McAfee, M.A., Baldwin, A.L., Wilson, L.M., 1998b. Identification and determination of material properties for porohyperelastic analysis of large arteries. J. Biomech. Eng. 120, 188–194.
Skrzypek, J., Ganczarski, A., 1999. Modeling of Material Damage and Failure of Structures. Springer, Berlin.
Tözeren, A., 1984. Elastic properties of arteries and their influence on the cardiovascular system. J. Biomech. Eng. 106, 182–185.
Truesdell, C., Noll, W., 2003. Non-Linear Field Theories of Mechanics, third ed. Springer, Heidelberg.
Vaishnav, R.N., Young, J.T., Patel, D.J., 1973. Distribution of stresses and of strain-energy density through the wall thickness in a canine aortic segment. Circ. Res. 32, 577–583.
Volokh, K.Y., 2004. Nonlinear elasticity for modeling fracture of isotropic brittle solids. J. Appl. Mech., ASME 71, 141–143.
Volokh, K.Y., 2006a. Compressibility of arterial wall in ring-cutting experiments. Mol. Cell. Biomech. 3, 35–42.
Volokh, K.Y., 2006b. Stresses in growing soft tissues. Acta Biomaterialia 2, 493–504.
Volokh, K.Y., 2007. Softening hyperelasticity for modeling material failure: analysis of cavitation in hydrostatic tension. Int. J. Solids Struct. 44, 5043–5055.

Volokh, K.Y., Gao, H., 2005. On the modified virtual internal bond method. J. Appl. Mech. 72, 969–971.

Volokh, K.Y., Ramesh, K.T., 2006. An approach to multi-body interactions in a continuum-atomistic context: application to analysis of tension instability in carbon nanotubes. Int. J. Solids Struct. 43, 7609–7627.

Wuyts, F.L., Vanhuyse, V.J., Langewouters, G.J., Decraemer, W.F., Raman, E.R., Buyle, S., 1995. Elastic properties of human aortas in relation to age and atherosclerosis: a structural model. Phys. Med. Biol. 40, 1577–1597.

Zhang, P., Klein, P., Huang, Y., Gao, H., Wu, P.D., 2002. Numerical simulation of cohesive fracture by the virtual-internal-bond method. Comput. Model. Eng. Sci. 3, 263–277.

Zhang, P., Jiang, H., Huang, Y., Geubelle, P.H., Hwang, K.C., 2004. An atomistic-based continuum theory for carbon nanotubes: analysis of fracture nucleation. J. Mech. Phys. Solids 52, 977–998.